ISSN 0915-633X

NATIONAL INSTITUTE FOR FUSION SCIENCE

Production of Negative Hydrogen Ions in a Large Multicusp Ion Source with Double-Magnetic Filter Configuration

A. Ando, Y. Takeiri, O. Kaneko, Y. Oka, M. Wada and T. Kuroda

(Received – Apr. 14, 1992)

NIFS-149 May 1992

RESEARCH REPORT
NIFS Series

NAGOYA, JAPAN

Production of negative hydrogen ions in a large multicusp ion source with double-magnetic filter configuration

A. Ando, Y. Takeiri, O. Kaneko, Y. Oka, M.Wada[a)] and T. Kuroda

National Institute for Fusion Science, Nagoya 464-01, Japan

ABSTRACT

The production of the negative hydrogen ions in a large multicusp ion source has been investigated in a double-magnetic filter (DMF) configuration. In the DMF configuration, the energetic electrons are trapped by the mirror of a magnetic multicusp field, and only the thermal electrons are present in the center of the arc chamber. A large amount of H^- ions of more than 1×10^{12} cm^{-3} are produced in the center region. The electron current extracted with the H^- ions can be suppressed by a magnetic filter field in front of a plasma grid without affecting the H^- ion current. The experimental data obtained in the DMF configuration are compared with those obtained in a single-magnetic filter (SMF) configuration. In the SMF configuration, the energetic electrons are present in the center region, and the magnetic filter in front of a plasma grid reduces the electron density and temperature, which results in the reduction of the H^- ion current as well as the electron current. The extracted electron current and the optimum gas pressure for the H^- ion current are lower in the DMF configuration than those in the SMF configuration.

KEYWORDS : negative ion source, H^- ion source, NBI, volume production, magnetic filter, photodetachment

I. INTRODUCTION

High power hydrogen/deuterium negative ion sources are urgently required for neutral beam injectors in application to fusion plasmas, because the negative ions of hydrogen isotopes (H^- or D^-) can be neutralized with high efficiencies to high-energy neutral beams with a very low divergence. Recent development of the negative hydrogen ion sources is concentrated on the volume production multicusp type[1-4], and the H^- ion current of several amperes has been obtained.[5] We have been also developing a multi-ampere negative hydrogen ion source, which is to be utilized for the negative-ion-based NBI system in the Large Helical Device (LHD) project in National Institute for Fusion Science (NIFS).[6,7] In recent experiments in NIFS, a 1.4A of H^- ion current has been obtained from a pure hydrogen discharge.[8,9]

In a volume source, a highly efficient H^- ion production is expected by a two-step process.[10,11] The first step is the vibrational excitation of hydrogen molecules by collisions with energetic electrons, the energy of which ε is more than 20eV, and the second is the dissociative attachment of slow electrons (ε=1 eV) to the exited molecules. It is important to separate the plasma into two regions where each process takes place, because the presence of electrons with energy larger than 2eV results in the collisional detachment of the produced H^- ions. In many multicusp H^- ion sources, an arc plasma is produced in the center of the arc chamber and the separation of these regions has been achieved by the magnetic filters such as external, rod, electromagnetic, and PG filters[5] generated in front of the plasma grid as shown in Fig. 1(a). In this configuration, which is called a single-magnetic filter (SMF) configuration hereinafter, the energetic electrons emitted from the filaments are confined in the center region by the cusp field, and excite the hydrogen molecules to higher

vibrational levels. The excited molecules H_2^* go through the magnetic filter and are dissociatively attached by the slow electrons in front of the plasma grid. The H^- ions are produced there and extracted from this region, which is called the extraction region. The magnetic filter reduces the electron density and temperature in the extraction region. Though the magnetic filter is advantageous for a suppression of the extracted electron current, a decrease in the electron density results in a reduction of the H^- ion production. Several methods are examined for the electron suppression with/without the magnetic filter.[12-14]

We have produced arc plasmas near the chamber wall, and the region separation has been realized by the cusp field. In this configuration, which is called a double-magnetic filter (DMF) configuration, the energetic electrons emitted from filaments are trapped by the mirror of the cusp field and only the slow electrons with low temperature of around 1eV are present in the center region as shown in Fig. 1(b). The vibrational excitation process occurs near the chamber wall and the dissociative attachment process occurs at the center region. Moreover, it is expected that the H_2^* production are enhanced by the collisions of H_2^+ and H_3^+ ions to the chamber wall.[15] We have also utilized the magnetic filter field in front of a plasma grid. It reduces the electron density in the extraction region. It is expected that the H^- ion production is not affected by the filter field and that the H^- ions produced in the center region go through the filter field and are extracted.

We have compared the DMF configuration with the conventional SMF configuration on the plasma parameters and on the H^- ion production in a large multicusp negative ion source. Spatial profiles of the electron density and temperature are measured in the two types of the filter configuration. The dependence of the plasma parameters and the H^- ion extraction

characteristics on an arc power and on a gas pressure are discussed. The electron energy distribution functions derived from probe measurements are described and the H^- ion densities measured by the photo-detachment technique are also presented.

II. EXPERIMENTAL DEVICES

A schematic diagram of the negative hydrogen ion source is shown in Fig. 2. This ion source is a rectangular magnetic-multipole type and has an extraction area of 25 × 25 cm^2. The cross section of the arc chamber is 35 × 35 cm^2 and its depth is 19 cm. Magnetic cusp lines in the arc chamber are generated by permanent magnet arrays arranged with 35 mm separation. The field strength is about 1 kGauss at the inner surface of the wall and decreases as the distance from the wall increases. Fourteen tungsten filaments of 1.5mm in diameter are attached at the side wall, and the distance between the wall and the filaments can be changed in order to modify the configurations.

The magnetic filter field in front of the plasma grid is generated by magnetic filter rods of 10mm in diameter and two external filter bars. The strength of the magnetic filter field can be changed by selecting the total number of the rods. The experiments have been done in the two cases of the filter strength, that is, number of the filter rods is 2 or 3. The magnetic field strengths between the filter rods are 26 and 46 Gauss, respectively. The distance between the plasma grid and the filter rods is set at 20 mm. The arc chamber and the filter rods are electrically connected and the plasma grid is floated to the arc chamber. Ports for Langmuir probes are provided so that the spatial scans (X and Z directions in Fig.2) of the probes can be made.

The negative ion extraction system consists of four grids as shown in Fig. 2. Each grid is made of copper and has 400 holes of 9 mm in diameter in the area of 25 × 25 cm^2 (transparency of 40 %). The plasma grid and the extraction grid have water cooling channels inside the grids. The extraction grid has also the channels to mount the permanent magnets to deflect the electrons extracted with H^- ions.

In the following experiments, the extraction voltage V_{ext} is set at 2 kV and the acceleration voltage V_{acc} is set at 3 kV. The electron suppression grid and the extraction grid are electrically connected. The beam pulse length is 0.3 sec.

The accelerated negative ions are measured by a calorimeter array which is placed at a distance of about 1.6 m downstream from the plasma grid. The array contains a series of seventeen calorimeters arranged in the X direction. The residual electrons accelerated with H^- ions are deflected by the magnetic field in front of the calorimeter. It is confirmed that no signal is detected in the He-discharge.

Profiles of the plasma parameters (the electron density and temperature) are measured by scanning Langmuir probes in the X and Z directions. The tip of the probe has a cylindrical shape of 2.0mm in length and 0.7mm in diameter. The probe voltage is scanned from -60V to +30V during 0.1sec with respect to the arc chamber. The time evolutions of the probe voltage and current are recorded by 10-bit digitizers and the plasma parameters are obtained from probe characteristic curves by using a computer.

The H^- ion density n^- is measured by the photodetachment technique using a Nd-YAG laser in the center region of the arc plasma. The probe is located inside the laser light path (wave length = 1.06μm, pulse length = 10ns,

power = 70mJ, beam diameter=7mm) and biased positively to collect the photodetached electrons.

III. EXPERIMENTAL RESULTS

A. Profiles of the arc plasma

In Figs. 3 (a) and (b) are shown the typical profiles in the X-direction of the electron temperature T_e and the electron density n_e in the DMF and SMF configurations, respectively. These profiles are measured by the Langmuir probe scanned in the X-direction at Z=85mm (Z=0 corresponds to the surface of the plasma grid).

The DMF and SMF configurations are realized by changing a filament position. When the filaments are located at 40mm apart from the wall, we have obtained the DMF configuration, where the profiles of T_e and n_e are hollow as shown in Fig. 3 (a). The cusp field strength at the filament position is 20 Gauss and emitted fast electrons are trapped near the chamber wall. T_e and n_e are higher in the peripheral region than those in the center region. The electron temperature is 7eV near the wall and decreases to about 1eV in the center region. The energetic electrons are not observed in the center region as discussed later. In the DMF configuration, the vibrationally excited hydrogen molecules (H_2^*) should be produced near the chamber wall. The negative hydrogen ions are produced in the center region by collisions between the H_2^* molecules and the slow electrons, and the produced H^- ions diffuse to the extraction region.

The SMF configuration is obtained when the filaments are set at 100mm apart from the wall. The profile of the arc plasma is flat as shown in Fig. 3 (b). The filaments are located at the field free region, and emitted fast electrons are confined in the center region of the arc chamber by the cusp field.

The bulk electron temperature T_e is about 3 eV and the probe characteristic curves show that the plasma in the center region contains the energetic electron component. The density n_e reaches about 3.0×10^{12} cm^{-3}. In the SMF configuration the H_2^* molecules should be produced in the center region.

Figures 4 (a) and (b) represent the profiles of T_e and n_e in the X direction at Z=5mm in the case of the DMF and SMF configurations, respectively. The profiles in the extraction region are nearly flat in both configurations in spite of the large discrepancy of the arc plasma profile in the center region. The temperatures T_e in the extraction region are 0.7eV in the DMF and 1.2eV in the SMF configuration.

The profiles of T_e and n_e in the Z-direction are shown in Figs. 5 (a) and (b) for the DMF and SMF configurations, respectively. The density n_e decreases as crossing the rod magnetic filter field in both configurations. Though the temperature T_e decreases from 3eV to 1eV in the SMF configuration, it does not seem to be much affected by the magnetic filter field in the DMF configuration. In the DMF configuration the magnetic filter field is utilized to control the electron density in the extraction region rather than the electron temperature. It is confirmed that T_e and n_e in the center region are not affected by the magnetic filter field strength.[8]

Figures 6 and 7 show the dependence of T_e and n_e on the input arc power P_{arc} in the DMF and SMF configurations, respectively. In the experiments, an arc voltage is changed simultaneously with an arc current in the range of V_{arc} = 45V-70V and I_{arc} = 200A-1400A. In the DMF configuration, n_e in the center and the extraction regions increase as P_{arc} increases as shown in Figs. 6 (a) and (b), respectively. However, T_e in the center region is almost constant around 1eV in spite of an increase in P_{arc}. These behaviors also indicate that

the energetic electrons generating the arc plasma are confined in the peripheral region in the DMF configuration. In the SMF configuration, T_e and n_e in the center region increase linearly with an increase in P_{arc} as shown in Fig.7 (a). In the extraction region, however, T_e is kept nearly constant below 1eV, though n_e increases as P_{arc} increases. (Fig. 7 (b))

Figures 8 and 9 show the dependence of T_e and n_e on the gas pressure in the DMF and SMF configurations, respectively. As the pressure increases, T_e in the center and the extraction regions decrease in both configurations (closed circles in Figs. 8 and 9). Though n_e in the center region is almost constant in both configurations, n_e in the extraction region decreases in the DMF configuration (Fig. 8(b)) and increases in the SMF configuration (Fig. 9(b)) as the pressure increases.

B. H^- ion extraction characteristics

The H^- ion extraction characteristics for the DMF and SMF configurations are shown in Figs.10 and 11, respectively. The H^- ion current densities measured by the central calorimeter J^-(calori.) and the extraction currents I_{ext} are plotted as a function of the arc power P_{arc} in the DMF configuration in Figs. 10 (a) and (b), respectively. For the low energy beams (the total acceleration voltage is 5kV), it is confirmed that the H^- ion beam profile is not much changed by the arc power. In the experiments, the total H^- ion current is about 1A at P_{arc}= 82kW. I_{ext} is considered to be the electron current extracted with the H^- ions. As P_{arc} increases, the H^- ion current increases linearly and I_{ext} increases more rapidly. The increase in I_{ext} corresponds to an increase in n_e in the extraction region. Though the H^- ion current is not affected by the rod magnetic filter field strength, I_{ext} decreases about 50% at P_{arc} = 50kW when the magnetic filter field is changed from 2-rods

to 3-rods. Therefore, it is found that the extracted electron current can be controlled by the magnetic filter field without affecting the H^- ion current in the DMF configuration. In the SMF configuration, J^-(calori.) and I_{ext} increase as P_{arc} increases as shown in Figs. 11 (a) and (b). When the magnetic filter field is changed from 2-rods to 3-rods, I_{ext} is suppressed about 50%, and J^-(calori.) decreases about 20% at P_{arc}=50kW. In the condition of the same J^-(calori.), I_{ext} in the DMF is lower than that in the SMF configuration.

The dependence of the H^- ion current densities and the extraction currents on the gas pressure in the DMF and SMF configurations are represented in Figs.12 and 13, respectively. As shown in Fig.12 (a), the optimum gas pressure for the H^- ion current is about 1.5Pa at P_{arc}=50kW in the DMF configuration, and the optimum pressure tends to be higher at higher arc power. It is remarkable that the extraction current decreases as the gas pressure increases as shown in Fig.12 (b). This corresponds to the decrease of the electron density in front of the plasma grid as shown in Fig.8 (b). In the SMF configuration, the H^- ion current becomes optimum at a higher pressure than that in the DMF configuration (Fig.13 (a)). Moreover, the extraction current increases as the pressure increases (Fig.13 (b)).

C. Electron energy distribution functions in the DMF configuration

For an effective H^- ion production in the volume source, it is important to separate the regions where vibrational excitations and the dissociative attachments occur. To confirm the region separation, that is, to know the localization of the energetic electrons in the DMF configuration, the electron energy distribution functions are derived from the probe measurements.

The electron energy distribution function f(E) is determined from the Druyvesteyn formula,[16]

$$f(E) = (2/S)(2mV)^{1/2}e^{-5/2}(d^2I/dV^2). \quad (1)$$

Here, I is the electron current to the probe, V is the probe potential with respect to the plasma potential, e and m are the charge and mass of an electron, and S is the probe area. The probe V-I curve is fitted by quadratic curves in succession[17] and the second derivative d^2I/dV^2 is derived from numerical calculations.

Figure 14 shows the electron energy distribution function f(E) obtained from Eq. (1). In the peripheral region (X=150mm), the plasma has an energetic component in the energy distribution function (Fig.14 (a)). From the logarithmic plot of $E^{-1/2}f(E)$ as shown in Fig. 14 (b), a lower temperature component of f(E) is fitted by T_e=5.2 eV and a higher temperature component is fitted by T_e=9.4eV. On the other hand, f(E) in the center region (X=2mm), shows no energetic component and is fitted by the Maxwellian distribution of T_e=0.92eV as shown in Figs.14 (c) and (d). These figures indicate that the energetic electrons emitted from filaments are localized near the chamber wall and that the only thermal electrons with their temperature around 1eV are present in the center region in the DMF configuration.

D. H^- ion density measurements by the photo-detachment technique

The H^- ion density in the arc plasma can be measured directly by the photo-detachment technique[18]. Preliminary measurements of the H^- ion density are made in the DMF configuration.

The positively-biased probe is inserted in the center of the arc chamber (Z=120mm), and irradiated by the Nd-YAG laser light. The photo-detached electrons from the H^- ions are detected as an increase in the electron saturation current I_{es}. No increase of I_{es} is observed in the He-discharge.

Figure 15 (a) shows the temporal evolution of I_{es} in the H_2-discharge. As shown in the figure, I_{es} increases abruptly when the laser light fires. It stays constant for about 0.6 μs and then decreases. The relative negative-ion density is determined from the ratio of the increment of I_{es} , ΔI_{es}, to the initial value of I_{es}, I_{es}^{init},

$$n^- / n_e = \Delta I_{es} / I_{es}^{init} \qquad (2)$$

The velocity of the H^- ions is estimated from the duration of the plateau of I_{es}, Δt_1,

$$V^- = (R - r) / \Delta t_1 \qquad (3)$$

where R is the radius of the laser beam (R=3.5mm), and r is the radius of the collection region (r is about 1mm).[19] It is found from Fig.15 (a) that the H^- ion density is almost the same as the electron density, and that the velocity of the H^- ions is roughly estimated to be 4×10^3 m/s. The measured H^- ion velocity is almost the same value as that in ref 19 and 20. The measured electron and the H^- ion densities are plotted as a function of the arc power and the gas pressure in Figs.15 (b) and (c), respectively. It is noted that the H^- ion density increases almost linearly with the arc power and reaches 1.7×10^{12} cm^{-3}. As the pressure increases, the H^- ion density increases and reaches the maximum ($n^- / n_e = 1$) at the pressure of 2.1Pa. The electron density in the center region, however, does not change as the pressure increases.

IV. DISCUSSION

In a plasma volume of a H^- ion source, the dominant process of the H^- ion production is the two-step process, that is, the vibrational excitation of hydrogen molecules and the dissociative attachment of slow electrons to the

vibrational excited molecules H_2^*. The H_2^* are produced in the ion source by several processes such as the fast electron collisions to the hydrogen molecules and the wall collisions of the positive ions (H_2^+ and H_3^+) to the wall.[21] In the SMF configuration, the H_2^* are produced mainly by the collisional excitation with energetic electrons in the center region of the arc chamber. In the DMF configuration, the excitation is expected to occur by the collisions of the energetic electrons near the filaments and possibly by the collisions of the positive ions to the wall. The H^- ions are produced by the dissociative attachment process in the center region, where the electron temperature is around 1eV which is sufficiently low for the attachment. The H^- ion density measurements indicate the high accumulation of H^- ions in the center region in the DMF configuration. This configuration is based on the similar operating principle to the hybrid source studied at Ecole Polytechnique[3,22,23] and the tent filter source at Culham Laboratory.[13,14]

Though the high density H^- ions are produced in the center region, they are easily destroyed by several processes before reaching the plasma grid. The dominant processes for the H^- ion destruction are as follows; (a) an electron detachment in collisions with electrons, (b) an electron detachment in collisions with neutral hydrogen molecules, (c) a mutual neutralization in collisions with positive ions (H^+, H_2^+ and H_3^+), and (d) an associative detachment in collisions with hydrogen atoms. In the center of the arc plasma in the DMF configuration, the electron temperature is around 1eV and the measured energy of the H^- ions is about 0.1eV. The H^- ion density is almost equal to the electron density of 1.5×10^{12} cm^{-3}. Since the reaction rate $\langle \sigma v \rangle$ of the process (a) is about 1×10^{-8} cm^3/s [24], the mean free path of the process (a) is about 30 cm. The process (b) is negligible, because the measured

energy of the H^- ions is lower than the threshold energy of the process (b).[25] The reaction rate $\langle\sigma v\rangle$ of the mutual neutralization between H^+ and H^- ions is about 2×10^{-8} cm^3/s [26-28], which can be used for the estimation of the H^- destruction by the process (c). The reaction rate of the process (d) is 20 times smaller than that of the process (c).[29,30] The prime process of the H^- destruction is process (c) and the mean free path of the H^- destruction is about 7cm. It is probable that the H^- ions produced in the center region diffuse to the extraction region. The H^- ions are also produced in the extraction region by the dissociative attachment. As shown in Fig.10, the extracted H^- ion current is not affected by the electron density in the extraction region. It indicates that the dissociative attachment occurs mainly in the center region in the DMF configuration.

In the photo-detachment experiments, there are some ambiguous points for the estimation of the H^- ion density. Since the cylindrical probe is inserted normally to the laser light, there is a shadow region around the probe tip. Moreover, since the signal detection system is not completely matched to the cable impedance, the signal is somewhat affected by the CR integration. Nevertheless, the above uncertainty leads to the under estimation of the H^- ion density, and it is confirmed that the high density H^- ions are produced in the center region in the DMF configuration.

The total H^- ion current of 1.2A is obtained at P_{arc} = 50kW when the acceleration voltage is set at 30kV.[9] It corresponds to the current density of 4.7 mA/cm^2, considering the total extraction area of 255 cm^2. Since the stripping loss in the accelerator is calculated at about 50%, the current density at the plasma grid is 10 mA/cm^2. However, the H^- ion current density in the center region can be estimated as $J^- = (1/4)\, en^-V^- = 24$ mA/cm^2, taking account of the

measured H^- ion density of 1.5×10^{12} cm^{-3} and the velocity of 4×10^5 cm/s. This value is two times larger than the above current density. This discrepancy may be due to the mutual neutralization of H^- ions before reaching the plasma grid.

V. CONCLUSIONS

The plasma parameters and the H^- ion extraction characteristics are measured in the DMF and SMF configurations and compared with each other.

In the DMF configuration the profiles of the electron density and temperature are hollow. The energetic electrons emitted from the filaments are trapped near the wall and there are only the thermal electrons with their temperature around 1eV in the center region. As the arc power increases, the electron density increases but the temperature is nearly constant in the center region. The extracted H^- ion and electron currents also increase linearly with the arc power. The extracted electron current increases correspondingly to an increase in the electron density in the extraction region and can be controlled by the magnetic filter field without affecting the H^- ion current.

On the other hand, the profiles of the electron density and temperature are flat, and the energetic electrons are contained in the center region in the SMF configuration. The electron temperature and density increase as the arc power increases. The magnetic filter field suppresses the H^- ion current as well as the electron current.

The advantages of the DMF configuration compared with the SMF configuration are as follows. The extracted electron current is lower in the DMF configuration than that in the SMF configuration in the same magnetic filter field strength. The optimum pressure for the H^- ion current is lower in

the DMF configuration than that in the SMF configuration. It is important to decrease the operating pressure, because high gas flow results in the large gas load to the pumping system and in the stripping loss of H^- ions in the accelerator.

The H^- ion density n^- are measured in the center region by the photo-detachment technique, and n^- of more than 1×10^{12} cm^{-3} is observed in the DMF configuration. This value is almost equal to the electron density. Both n_e and n^- increase linearly with keeping the ratio $n^-/n_e = 1$ as the arc power increases.

ACKNOWLEDGMENTS

The authors would like to thank Dr. A.J.T.Holmes, Dr. J.R.Hiskes and Dr. F.Sano for their useful discussions. The authors would also like to thank K. Mineo, R. Akiyama, T. Kawamoto and A. Karita for their help in the experiments.

REFERENCES

a)Permanent address; Faculty of Engineering, Doshisha University, Kyoto, 602, Japan.

1) K.N.Leung, C.A.Hauck, W.B.Kunkel, and S.R.Walther, Rev. Sci. Instrum. **60**, 531 (1989).

2) A.J.T.Holmes, L.M.Lea, A.F.Newman, and M.P.S. Nightingale, Rev. Sci. Instrum. **58**, 223 (1987).

3) M.Bacal, J.Bruneteau, and P.Devynck, Rev. Sci. Instrum. **59**, 2152 (1988).

4) T. Inoue, M. Araki, M. Hanada, T.Kurashima, S.Matsuda, et. al., Nucl. Instr. Meth. **B37/38**, 111 (1989).

5) M.Hanada, T.Inoue, H.Kojima, Y.Matuoka, Y.Ohara, et. al. Rev. Sci. Instrum. **61**, 499 (1990).

6) A.Iiyoshi, Proc. of the 13th Symp. on Fusion Engineering, Knoxville, 1989, p. 1007.

7) O.Motojima, K.Akaishi, M.Asao, K.Fujii, J.Fujita, et. al., Proc. the 13th Inter. Conf. on Plasma Physics and Controlled Nuclear Fusion Research, Washington, DC, 1990, paper No. IAEA-CN-53/G-1-5.

8) Y.Takeiri, A.Ando, O.Kaneko, Y.Oka, R.Akiyama, et. al., Proc. of the 16th Symp. on Fusion Technology, London, 1990, (to be published).

9) Y.Takeiri, A.Ando, O.Kaneko, Y.Oka, and T.Kuroda, (to be submitted).

10) J.M.Wadehra, and J.N.Berdsley, Phys. Rev. Lett. **41**. 1795 (1978).

11) J.R.Hiskes, and A.M.Karo, J. Appl. Phys. **56**, 1927 (1984).

12) K.N.Leung, C.A.Hauck, W.B.Kunkel, and S.R.Walther, Rev. Sci. Instrum. **61**, 1110 (1990).

13) L.M.Lea, A.J.T.Holmes, M.F.Thornton, and G.O.R.Naylor, Rev. Sci. Instrum. **61**, 409 (1990).

14) R.McAdams, R.F.King, and A.F.Newman, Rev. Sci. Instrum. **61**, 2176

(1990).

15) J.R.Hiskes, and A.M.Karo, J. Appl. Phys. **67**, 6621 (1990).

16) J.M.Druyvesteyn, Z. Phys. **64**, 781 (1930).

17) F.Fujita, and H.Yamazaki, Jpn. J. Appl. Phys. **29**, 2139 (1990).

18) M.Bacal, and G.W.Hamilton, Phys. Rev. Lett. **42**, 1538 (1979).

19) P.Devynck, J.Anvray, M.Bacal, P.Berlemont, J.Bruneteau, R.Leroy, and A.Stern, Rev. Sci. Instrum. **60**, 2873 (1989).

20) P.J.Eenshuistra, M.Gochitashvilli, R.Becker, A.W.Kleyn, and H.J.Hopman, J. Appl. Phys. **67**, 85 (1990).

21) J.R.Hiskes, Appl. Phys. Lett. **57**, 231 (1990).

22) M.Bacal, A.M. Bruneteau, and M. Nachman, J. Appl. Phys. **55**, 15 (1984).

23) M.Bacal, F.Hillion, and M.Nachman, Rev. Sci. Instrum. **56**, 649 (1985).

24) D.S.Walton, B.Peart, and K.T.Dolder, J. Phys. **B4**, 1343 (1971).

25) M.S.Huq, L.D.Doverspike, and R.L.Champion, Phys. Rev. **A27**, 2831 (1983),

26) S.Szucs, M.Karemera, M.Terao, and F.Brouillard, J. Phys. **B17**, 1613 (1984).

27) B.Peart, M.A.Bennett, and K.Dolder, J. Phys. **B18**, L439 (1985).

28) D.Fussen, and C.Kubach, J. Phys. **B19**, L31 (1986).

29) R.J.Bieniek, and A.Dalgarno, Astrophys. J. **228**, 635 (1979).

30) R.K.Janev, and A.R.Tancic, J. Phys. **B4**, 219 (1971).

FIGURE CAPTIONS

Fig. 1

Figures illustrating the concepts of (a) the SMF configuration and (b) the DMF configuration. Hatched regions represent the hot plasmas containing energetic electrons. Cusp fields are indicated by arrows.

Fig. 2

The schematic diagram of the multicusp negative hydrogen ion source.

Fig. 3

The profiles of n_e (open circles) and T_e (closed circles) in the X-direction (a) in the DMF configuration and (b) in the SMF configuration. Positions of the filaments and the wall are indicated by arrows. The probe is scanned in the X-direction at Z=85mm. The gas pressure is 1.9Pa. P_{arc}=46 kW.

Fig. 4

The profiles of n_e (open circles) and T_e (closed circles) in the X-direction (a) in the DMF configuration and (b) in the SMF configuration. The probe is scanned in the X-direction at Z=5mm. The gas pressure is 1.9Pa. P_{arc}=46 kW.

Fig. 5

The profiles of n_e (open circles) and T_e (closed circles) in the Z-direction (a) in the DMF configuration and (b) in the SMF configuration for the 2-rods magnetic filter. An arrow and a circle indicate positions of the plasma grid and the filter rods, respectively. The gas pressure is 1.9Pa. P_{arc}=45 kW.

Fig. 6

The dependence of n_e (open circles) and T_e (closed circles) on the arc power P_{arc} in the DMF configuration. The probe is set (a) in the center region (Z=90mm) and (b) in the extraction region (Z=5mm) for the 3-rods magnetic filter. The gas pressure is 1.9Pa.

Fig. 7

The dependence of n_e (open circles) and T_e (closed circles) on the arc power P_{arc} in the SMF configuration. The probe is set (a) in the center region (Z=90mm) and (b) in the extraction region (Z=5mm) for the 3-rods magnetic filter. The gas pressure is 1.9Pa.

Fig. 8

The dependence of n_e (open circles) and T_e (closed circles) on the gas pressure in the DMF configuration. The probe is set (a) in the center region (Z=90mm) and (b) in the extraction region (Z=5mm) for the 3-rods magnetic filter. P_{arc}=45 kW.

Fig. 9

The dependence of n_e (open circles) and T_e (closed circles) on the gas pressure in the SMF configuration. The probe is set (a) in the center region (Z=90mm) and (b) in the extraction region (Z=5mm) for the 3-rods magnetic filter. P_{arc}=45 kW.

Fig. 10

(a) J^- (calori.) and (b) I_{ext} as a function of P_{arc} for the 3-rods magnetic filter (open circles) and for the 2-rods magnetic filter (closed circles) in the DMF

configuration. The gas pressure is 1.9Pa.

Fig. 11

(a) J^- (calori.) and (b) I_{ext} as a function of P_{arc} for the 3-rods magnetic filter (open circles) and for the 2-rods magnetic filter (closed circles) in the SMF configuration. The gas pressure is 1.9Pa.

Fig. 12

(a) J^- (calori.) and (b) I_{ext} as a function of the filling gas pressure for the 3 rods magnetic filter in the DMF configuration. Parameter is the arc power.

Fig. 13

(a) J^- (calori.) and (b) I_{ext} as a function of the filling gas pressure for the 3 rods magnetic filter in the SMF configuration. Parameter is the arc power.

Fig. 14

The electron energy distribution function derived from the probe characteristic curve measured at X=150mm in (a) and (b), and at X=2mm in (c) and (d). The gas pressure is 1.9Pa. Z=85mm. P_{arc}=45kW.

Fig. 15

(a) The time evolution of the electron saturation current I_{es}. The YAG laser pulse is indicated by an arrow. The probe is set at Z=120mm and its bias voltage is +20V. The gas pressure is 2.1Pa and P_{arc}=43kW. The dependence of the H^- ion density n^- (closed circles) and the electron density (open circles) (b) on the arc power and (c) on the gas pressure.

(a) The SMF configuration

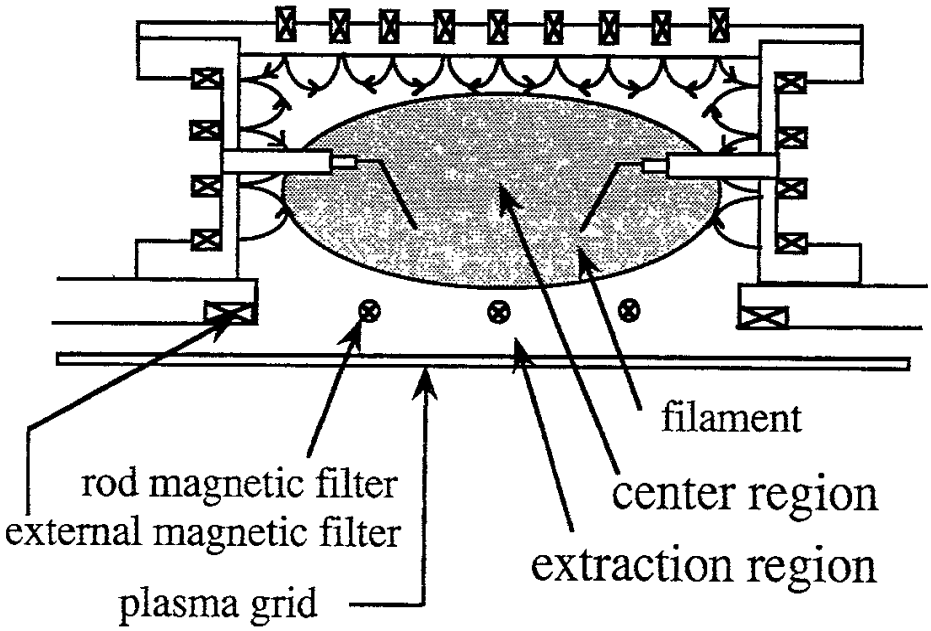

(b) The DMF configuration

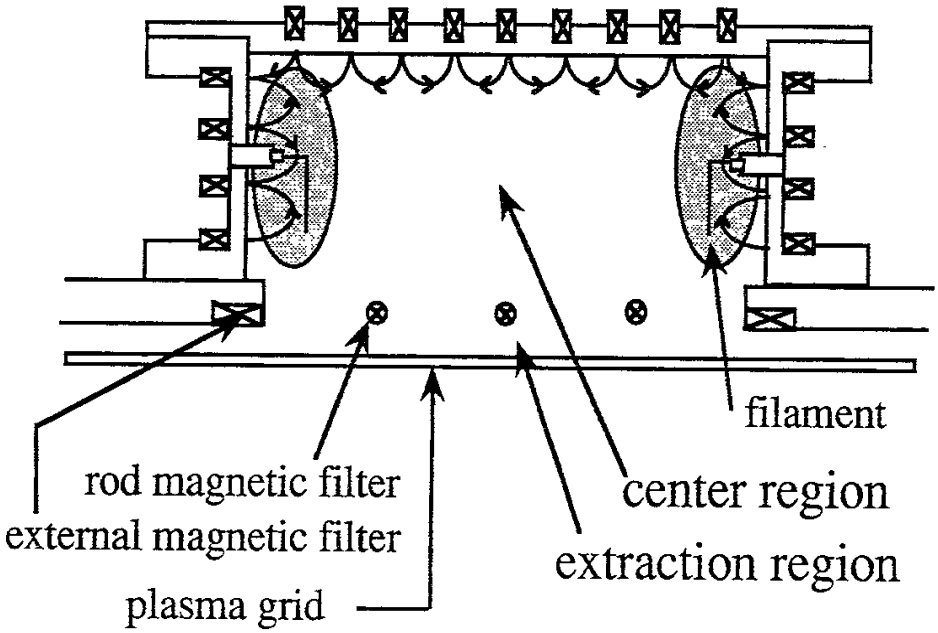

Fig. 1

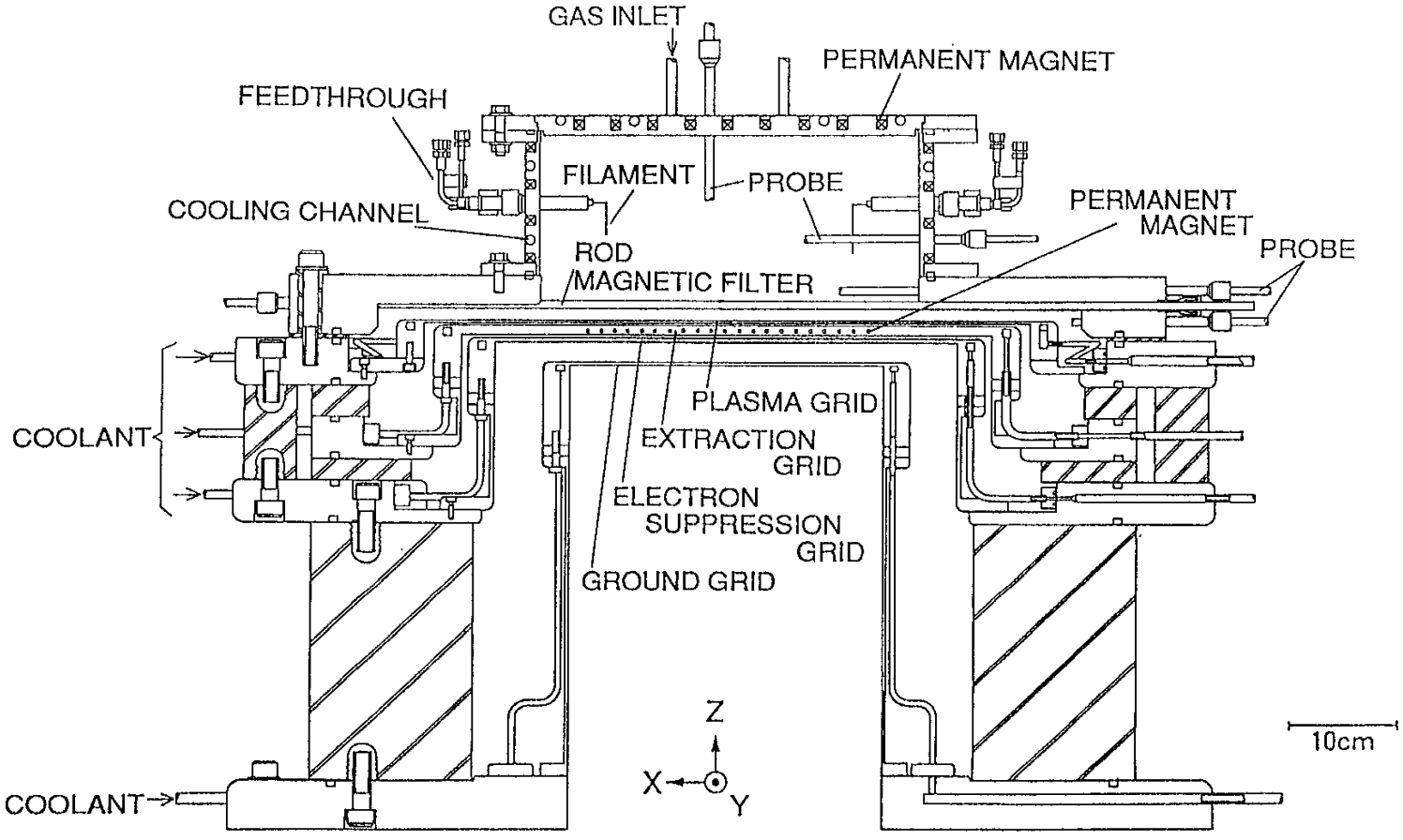
GAS INLET
PERMANENT MAGNET
FEEDTHROUGH
FILAMENT
PROBE
COOLING CHANNEL
PERMANENT MAGNET
PROBE
ROD
MAGNETIC FILTER
PLASMA GRID
COOLANT
EXTRACTION GRID
ELECTRON SUPPRESSION GRID
GROUND GRID
Z
X
Y
10cm
COOLANT

Fig. 2

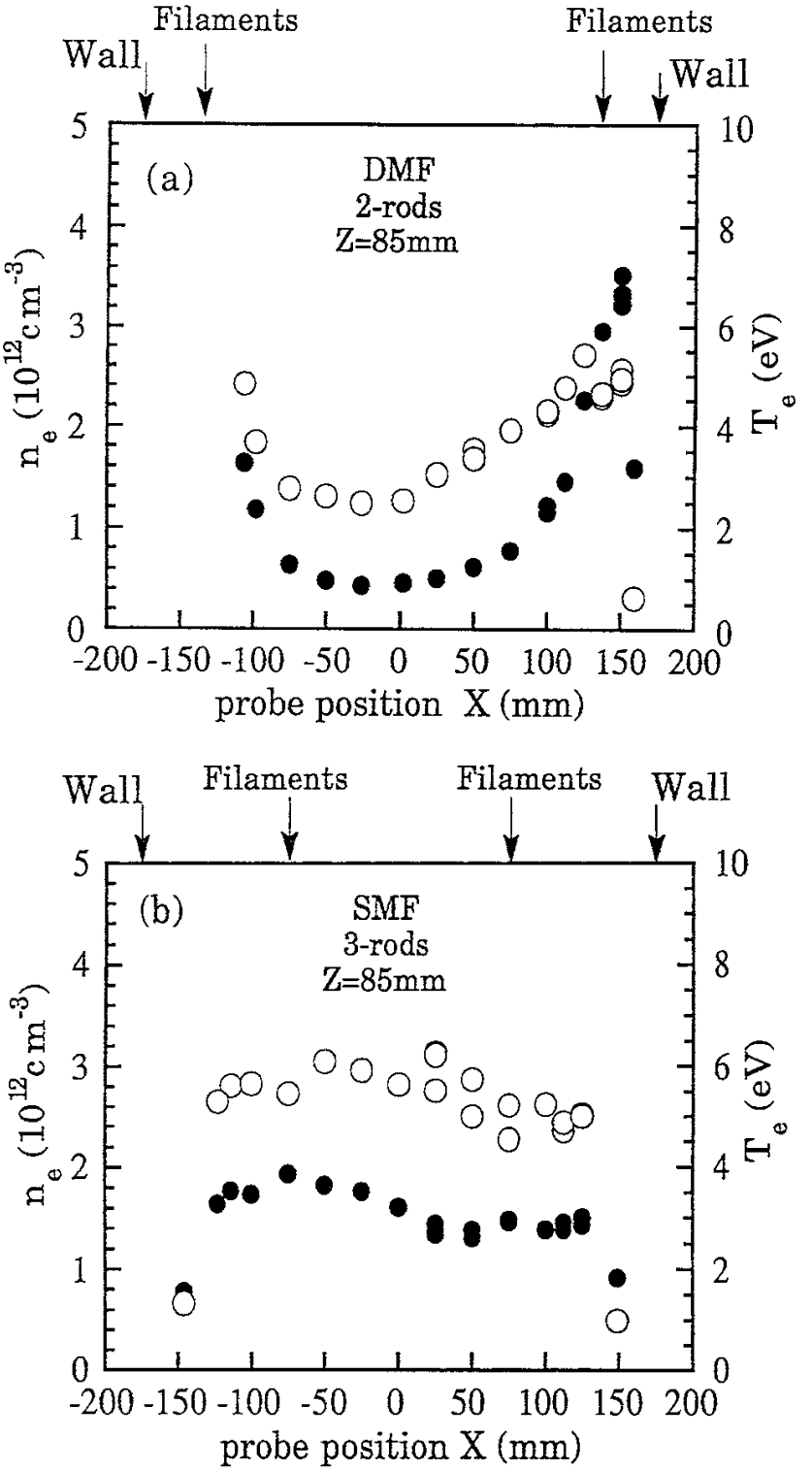
Wall
Filaments
Filaments
Wall
(a)
DMF
2-rods
Z=85mm
n_e (10^{12}cm^{-3})
T_e (eV)
probe position X (mm)
(b)
SMF
3-rods
Z=85mm
n_e (10^{12}cm^{-3})
T_e (eV)
probe position X (mm)

Fig. 3

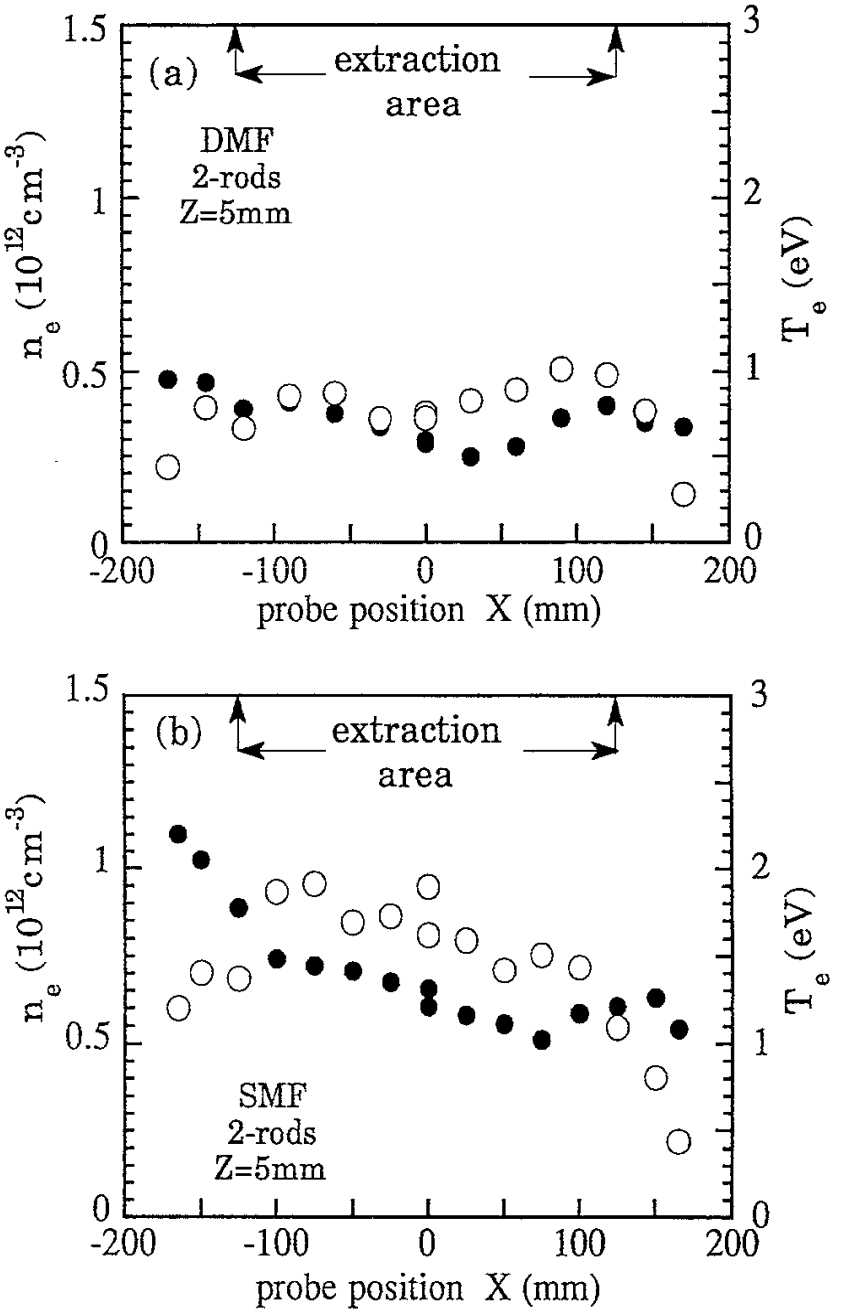
(a)
extraction area
DMF
2-rods
Z=5mm
n_e (10^{12}cm^{-3})
T_e (eV)
probe position X (mm)
(b)
extraction area
SMF
2-rods
Z=5mm
n_e (10^{12}cm^{-3})
T_e (eV)
probe position X (mm)

Fig. 4

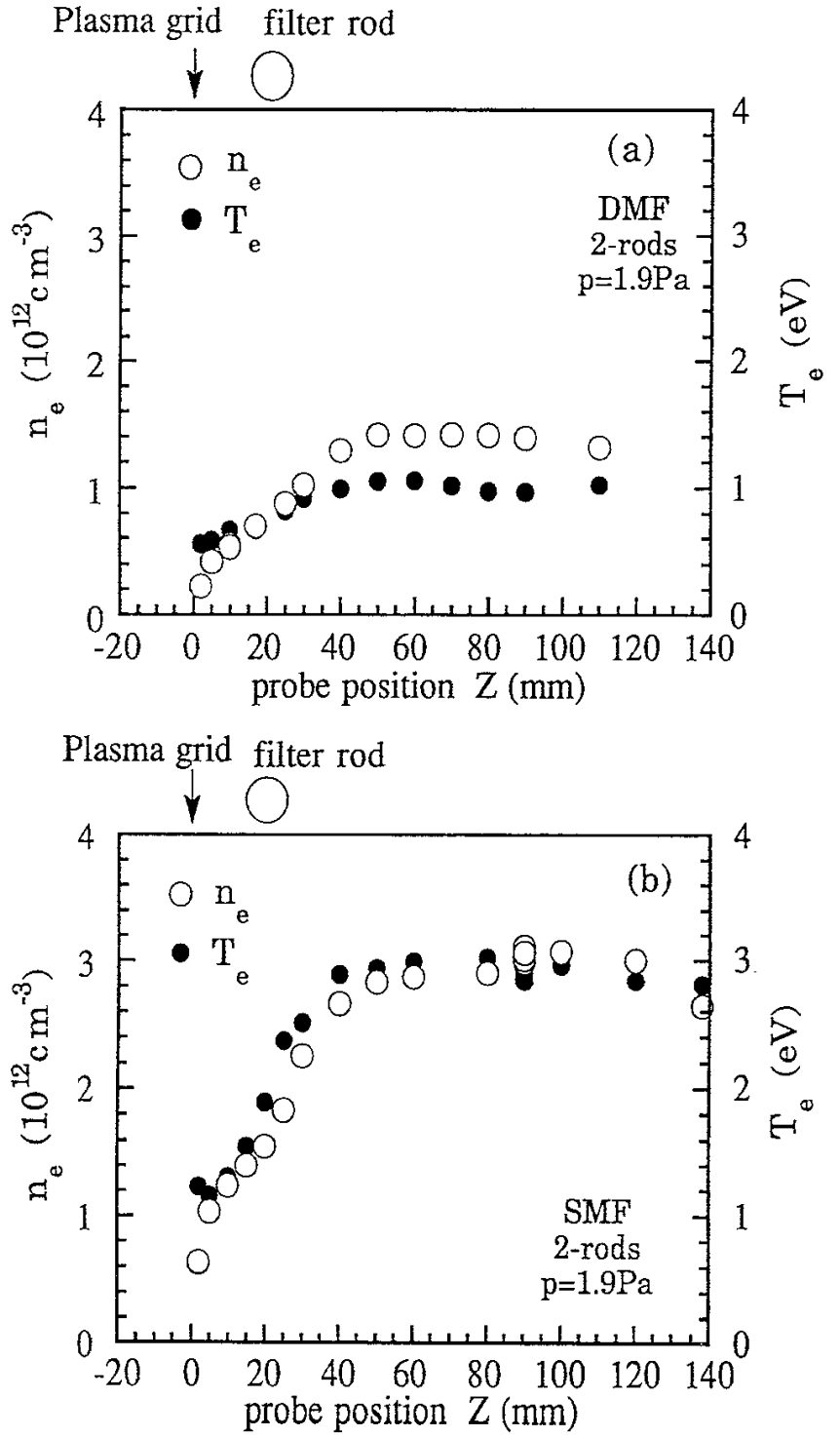
Plasma grid
filter rod
(a)
n_e
T_e
DMF
2-rods
p=1.9Pa
n_e (10^{12}cm^{-3})
T_e (eV)
probe position Z (mm)
Plasma grid
filter rod
(b)
n_e
T_e
SMF
2-rods
p=1.9Pa
n_e (10^{12}cm^{-3})
T_e (eV)
probe position Z (mm)

Fig. 5

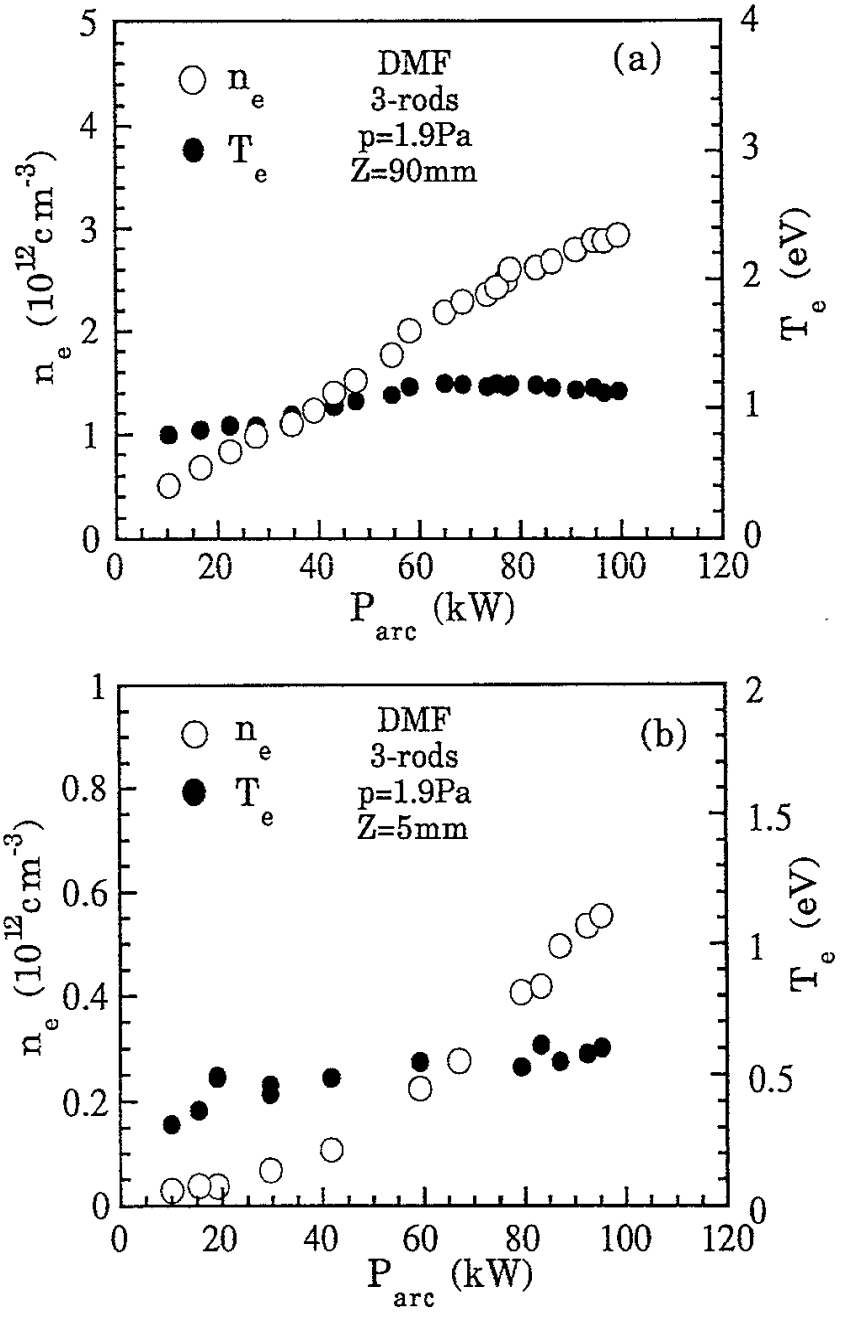
DMF
3-rods
p=1.9Pa
Z=90mm
(a)
n_e
T_e
n_e (10^12 cm^-3)
T_e (eV)
P_arc (kW)
DMF
3-rods
p=1.9Pa
Z=5mm
(b)
n_e
T_e
n_e (10^12 cm^-3)
T_e (eV)
P_arc (kW)

Fig. 6

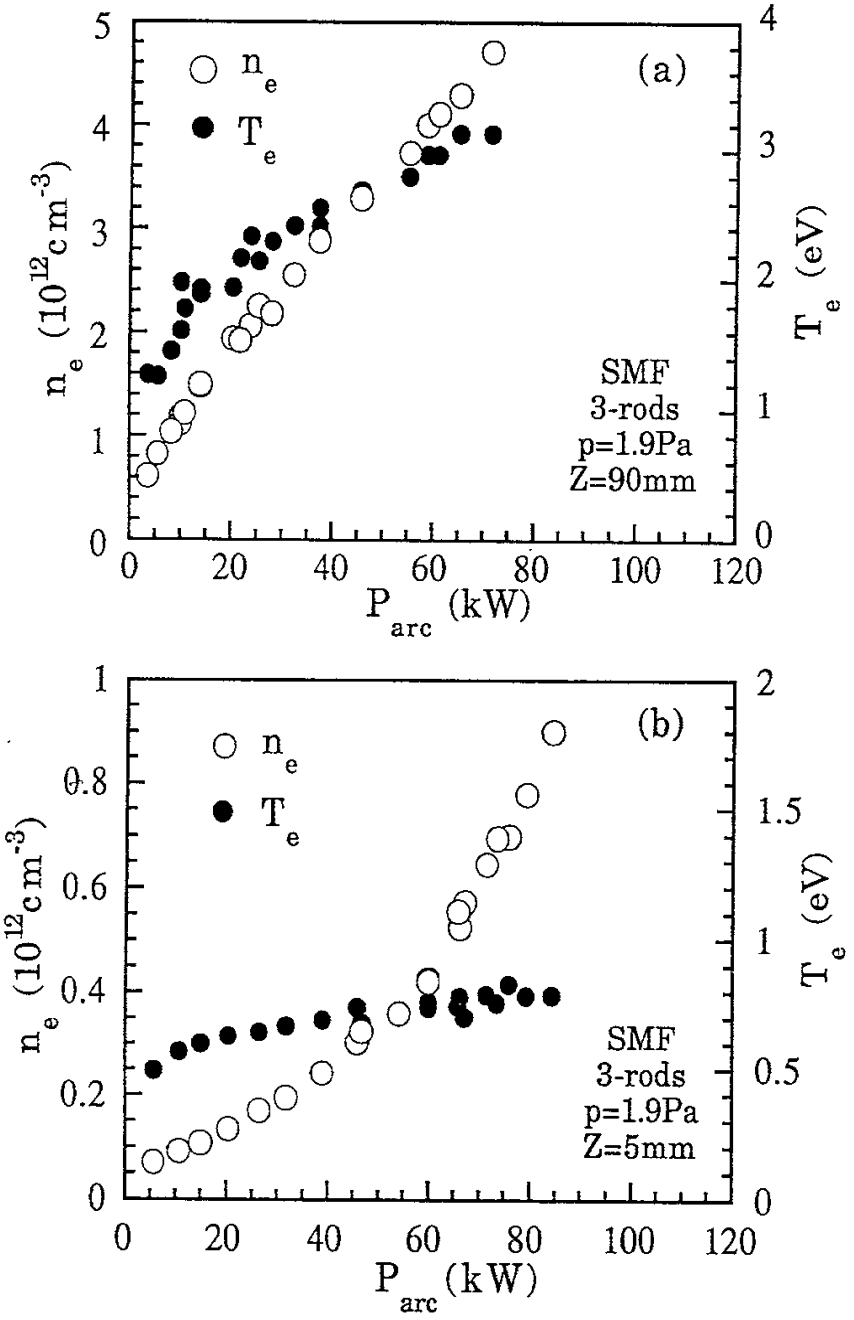
(a)
n_e
T_e
SMF
3-rods
p=1.9Pa
Z=90mm
n_e (10^12 cm^-3)
T_e (eV)
P_arc (kW)
0
20
40
60
80
100
120
1
2
3
4
5
(b)
n_e
T_e
SMF
3-rods
p=1.9Pa
Z=5mm
n_e (10^12 cm^-3)
T_e (eV)
P_arc (kW)
0.2
0.4
0.6
0.8
0.5
1.5

Fig. 7

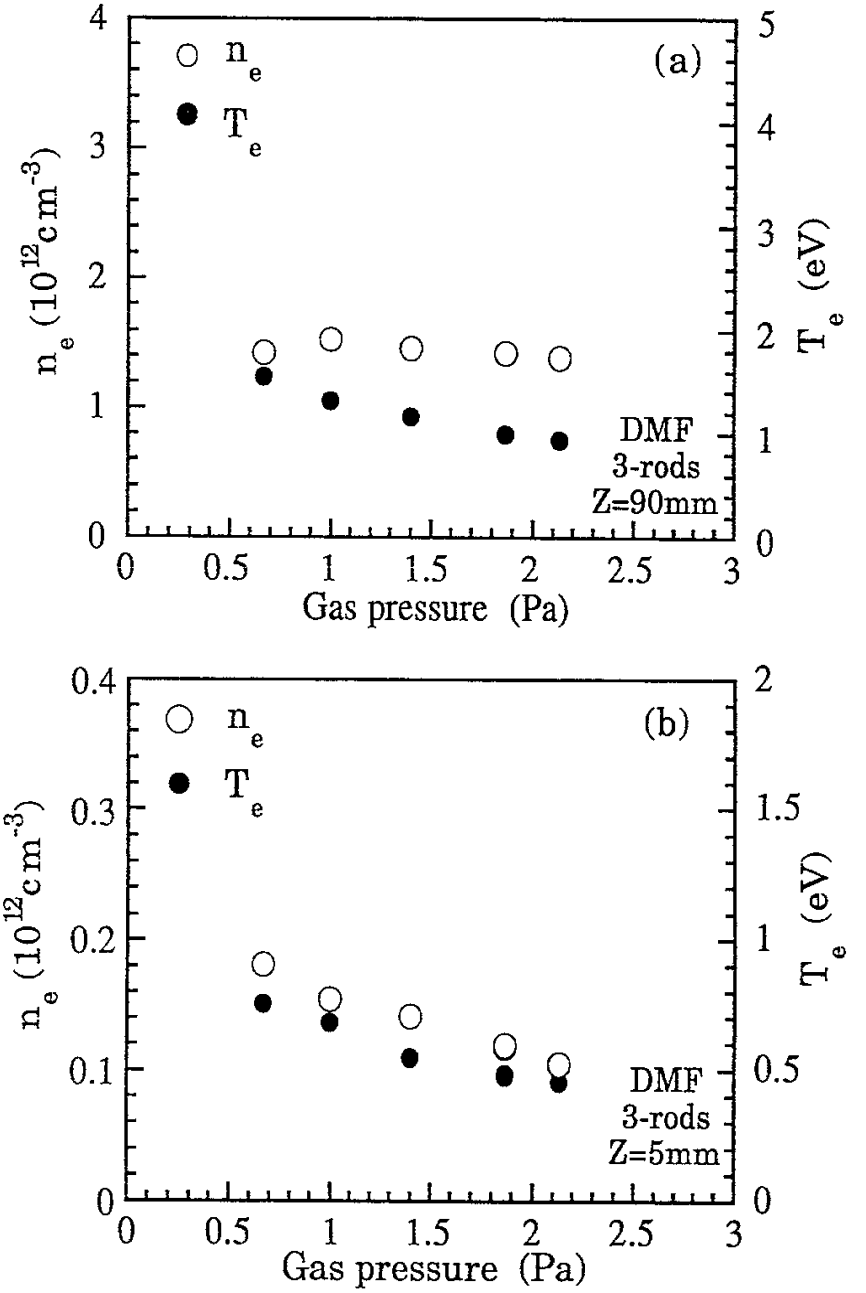
(a)
n_e
T_e
DMF
3-rods
Z=90mm
n_e (10^{12}cm^{-3})
T_e (eV)
Gas pressure (Pa)
(b)
n_e
T_e
DMF
3-rods
Z=5mm
n_e (10^{12}cm^{-3})
T_e (eV)
Gas pressure (Pa)

Fig. 8

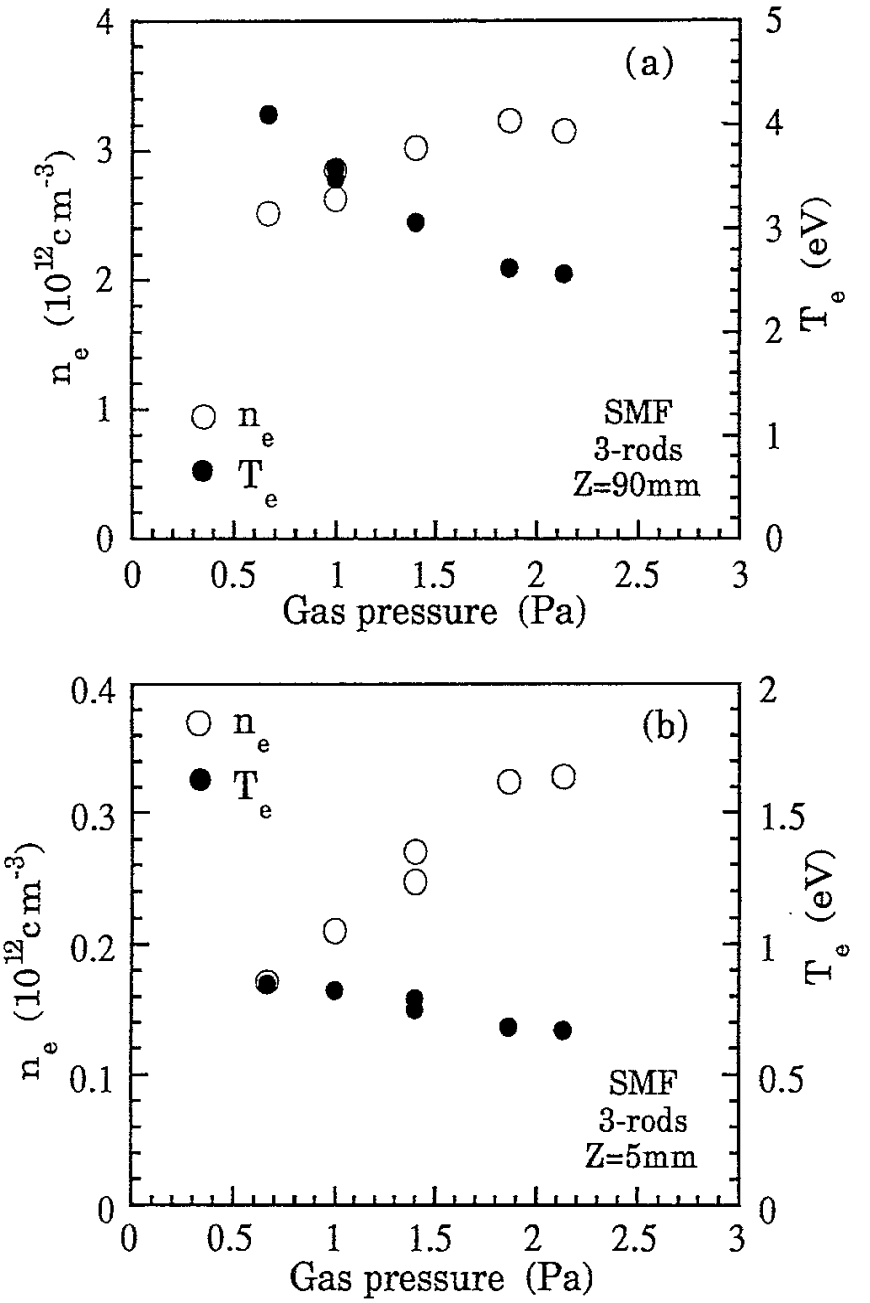
(a)
n_e
T_e
SMF
3-rods
Z=90mm
n_e (10^{12} c m^{-3})
T_e (eV)
Gas pressure (Pa)
(b)
n_e
T_e
SMF
3-rods
Z=5mm
n_e (10^{12} c m^{-3})
T_e (eV)
Gas pressure (Pa)

Fig. 9

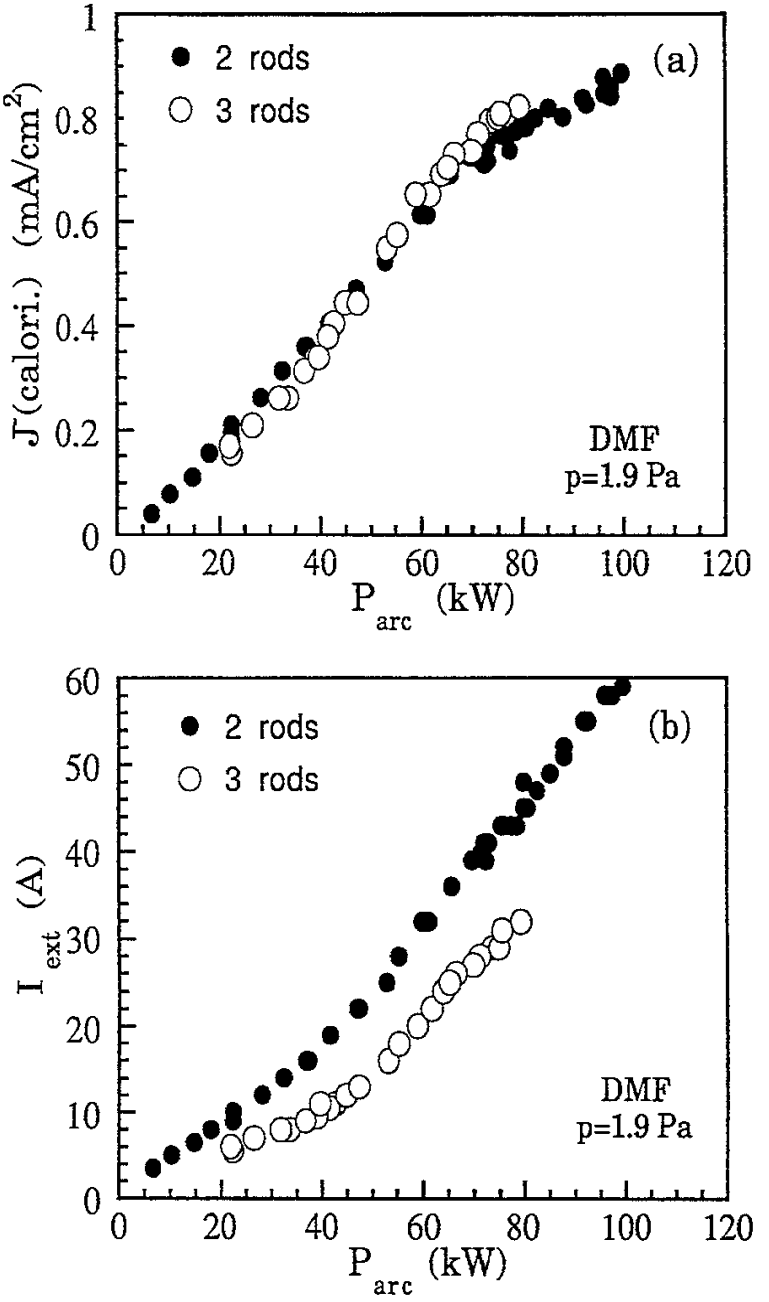
1
0.8
0.6
0.4
0.2
0
J(calori.) (mA/cm^2)
2 rods
3 rods
(a)
DMF
p=1.9 Pa
0
20
40
60
80
100
120
P$_{arc}$ (kW)
60
50
40
30
20
10
0
I$_{ext}$ (A)
2 rods
3 rods
(b)
DMF
p=1.9 Pa
0
20
40
60
80
100
120
P$_{arc}$ (kW)

Fig. 10

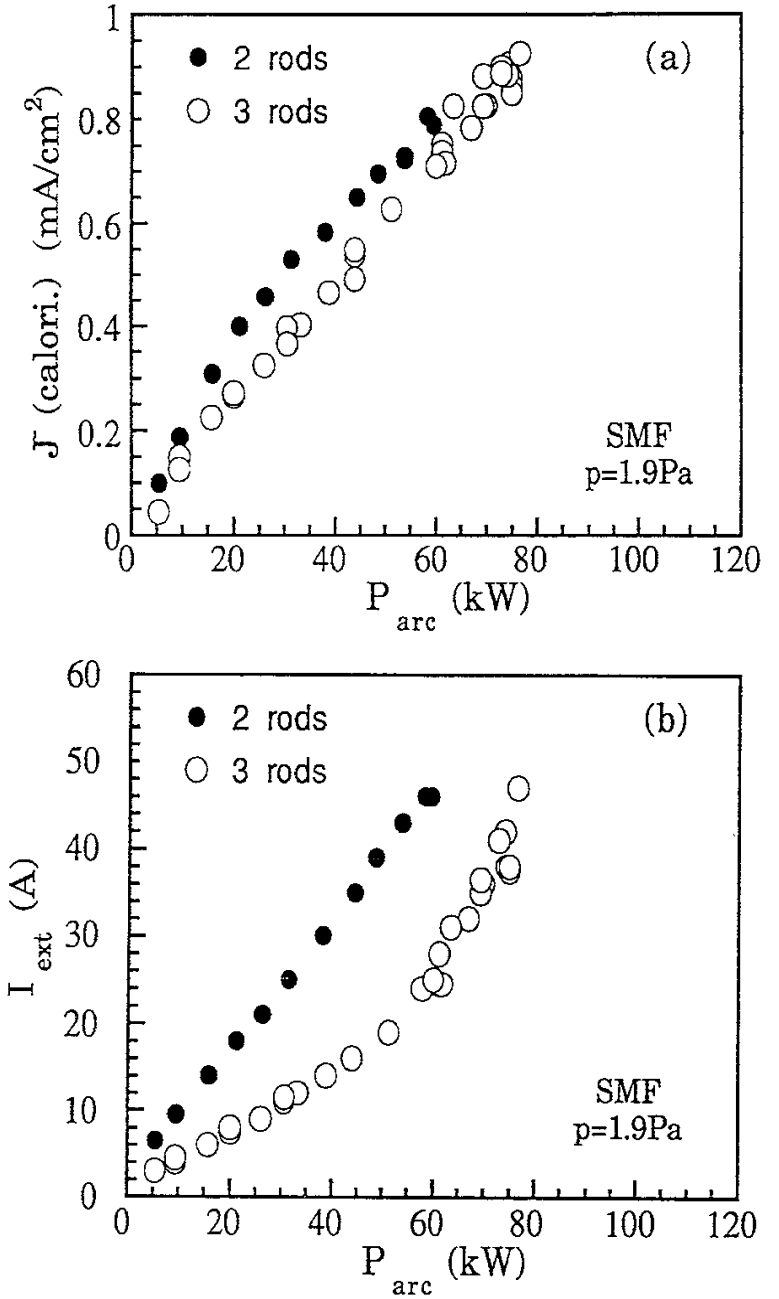
2 rods
3 rods
(a)
SMF
p=1.9Pa
J (calori.) (mA/cm^2)
P_{arc} (kW)
0
0.2
0.4
0.6
0.8
1
0
20
40
60
80
100
120
2 rods
3 rods
(b)
SMF
p=1.9Pa
I_{ext} (A)
P_{arc} (kW)
0
10
20
30
40
50
60
0
20
40
60
80
100
120

Fig. 11

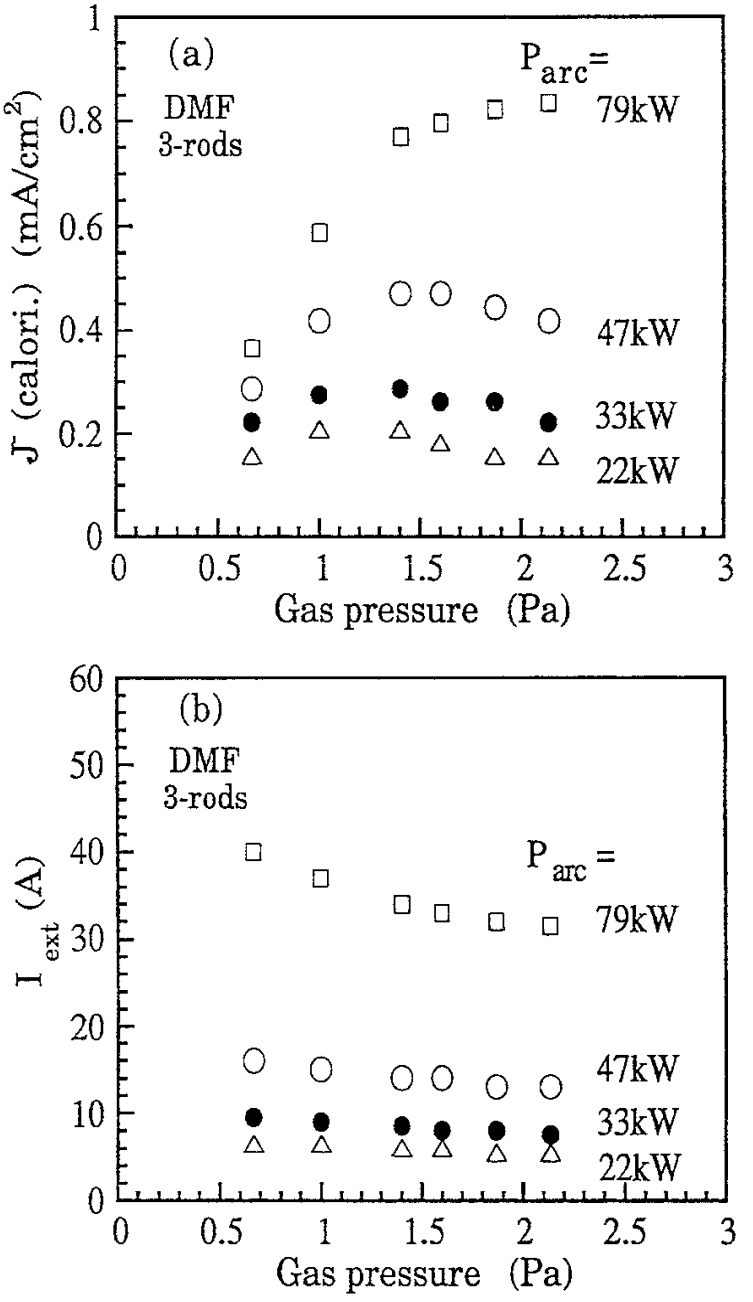
(a)
DMF
3-rods
P_{arc}=
79kW
47kW
33kW
22kW
J (calori.) (mA/cm^2)
Gas pressure (Pa)
(b)
DMF
3-rods
P_{arc} =
79kW
47kW
33kW
22kW
I_{ext} (A)
Gas pressure (Pa)

Fig. 12

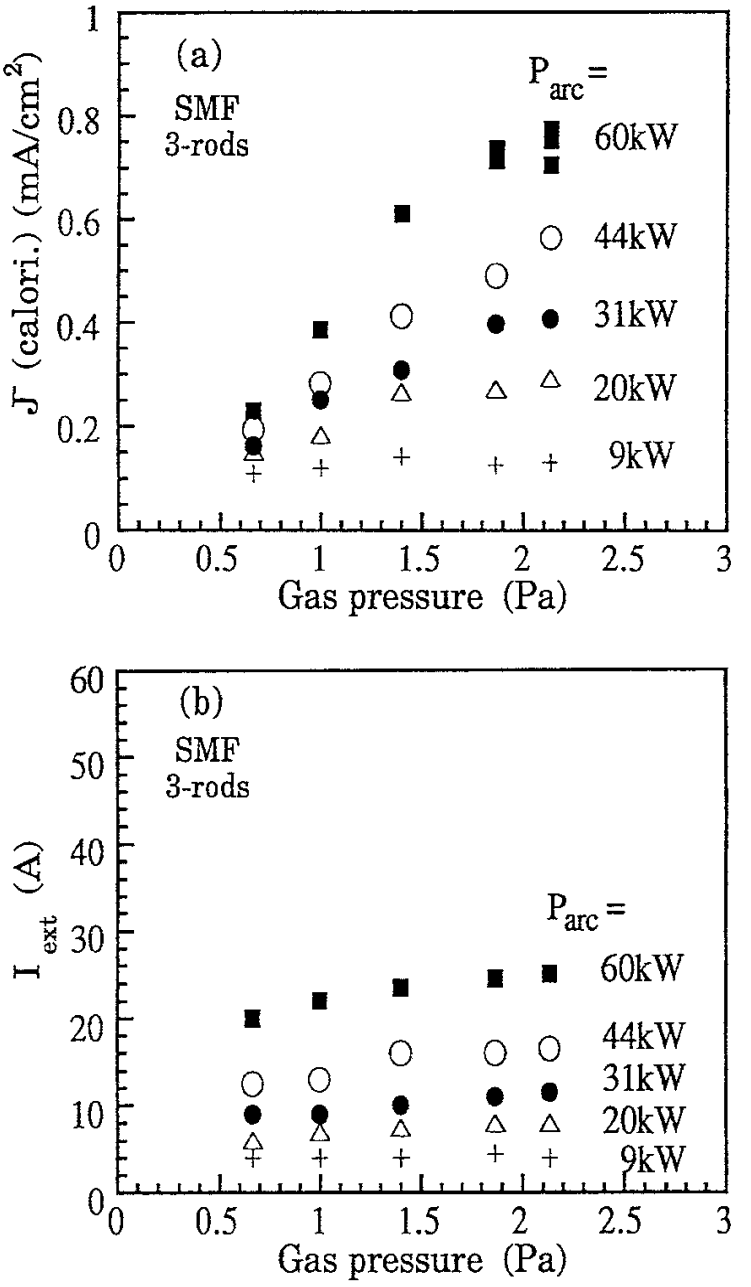
(a)
SMF
3-rods
P_{arc} =
60kW
44kW
31kW
20kW
9kW
J (calori.) (mA/cm^2)
Gas pressure (Pa)
(b)
SMF
3-rods
P_{arc} =
60kW
44kW
31kW
20kW
9kW
I_{ext} (A)
Gas pressure (Pa)

Fig. 13

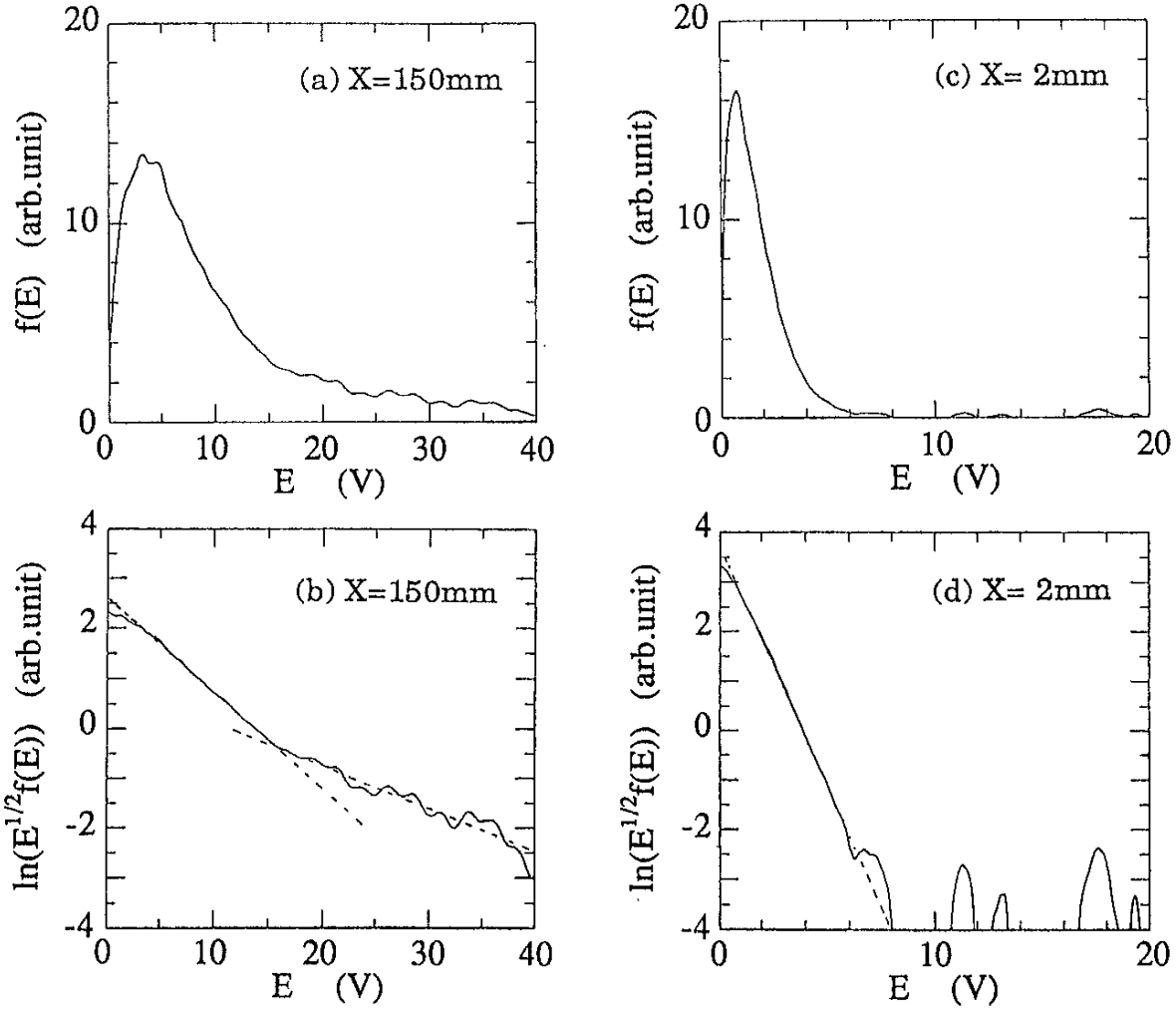
(a) X=150mm
f(E) (arb.unit)
E (V)
(c) X= 2mm
f(E) (arb.unit)
E (V)
(b) X=150mm
ln(E^1/2 f(E)) (arb.unit)
E (V)
(d) X= 2mm
ln(E^1/2 f(E)) (arb.unit)
E (V)

Fig. 14

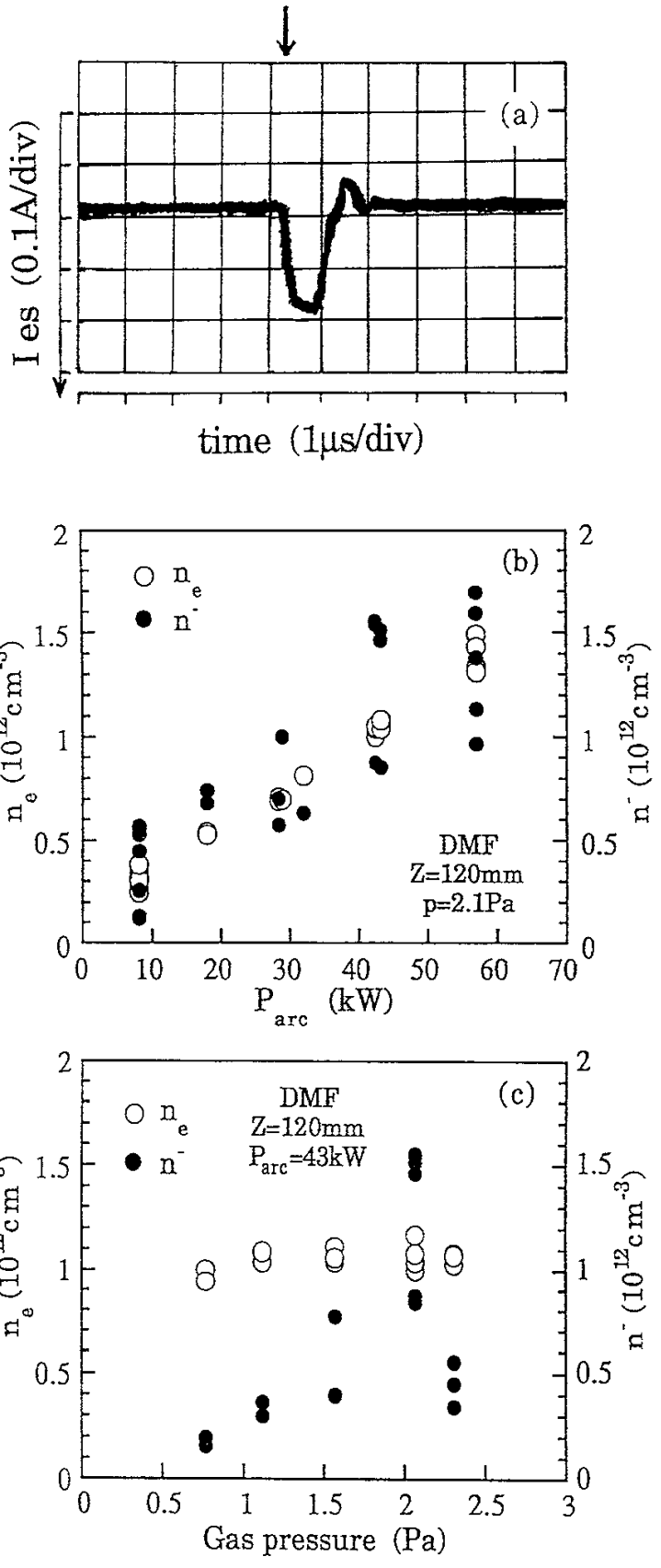
(a)
I es (0.1A/div)
time (1μs/div)
(b)
n_e
n^-
DMF
Z=120mm
p=2.1Pa
n_e (10^12 cm^-3)
n^- (10^12 cm^-3)
P_arc (kW)
(c)
DMF
Z=120mm
P_arc=43kW
Gas pressure (Pa)

Fig. 15

Recent Issues of NIFS Series

NIFS-98 H. Hojo, T. Watanabe, M. Inutake, M. Ichimura and S. Miyoshi, *Axial Pressure Profile Effects on Flute Interchange Stability in the Tandem Mirror GAMMA 10;* Jun. 1991

NIFS-99 A. Usadi, A. Kageyama, K. Watanabe and T. Sato, *A Global Simulation of the Magnetosphere with a Long Tail : Southward and Northward IMF;* Jun. 1991

NIFS-100 H. Hojo, T. Ogawa and M. Kono, *Fluid Description of Ponderomotive Force Compatible with the Kinetic One in a Warm Plasma* ; July 1991

NIFS-101 H. Momota, A. Ishida, Y. Kohzaki, G. H. Miley, S. Ohi, M. Ohnishi K. Yoshikawa, K. Sato, L. C. Steinhauer, Y. Tomita and M. Tuszewski *Conceptual Design of D-^{3}He FRC Reactor "ARTEMIS"* ; July 1991

NIFS-102 N. Nakajima and M. Okamoto, *Rotations of Bulk Ions and Impurities in Non-Axisymmetric Toroidal Systems* ; July 1991

NIFS-103 A. J. Lichtenberg, K. Itoh, S. - I. Itoh and A. Fukuyama, *The Role of Stochasticity in Sawtooth Oscillation* ; Aug. 1991

NIFS-104 K. Yamazaki and T. Amano, *Plasma Transport Simulation Modeling for Helical Confinement Systems;* Aug. 1991

NIFS-105 T. Sato, T. Hayashi, K. Watanabe, R. Horiuchi, M. Tanaka, N. Sawairi and K. Kusano, *Role of Compressibility on Driven Magnetic Reconnection ;* Aug. 1991

NIFS-106 Qian Wen - Jia, Duan Yun - Bo, Wang Rong - Long and H. Narumi, *Electron Impact Excitation of Positive Ions - Partial Wave Approach in Coulomb - Eikonal Approximation* ; Sep. 1991

NIFS-107 S. Murakami and T. Sato, *Macroscale Particle Simulation of Externally Driven Magnetic Reconnection;* Sep. 1991

NIFS-108 Y. Ogawa, T. Amano, N. Nakajima, Y. Ohyabu, K. Yamazaki, S. P. Hirshman, W. I. van Rij and K. C. Shaing, *Neoclassical Transport Analysis in the Banana Regime on Large Helical Device (LHD) with the DKES Code;* Sep. 1991

NIFS-109 Y. Kondoh, *Thought Analysis on Relaxation and General Principle to Find Relaxed State;* Sep. 1991

NIFS-110 H. Yamada, K. Ida, H. Iguchi, K. Hanatani, S. Morita, O. Kaneko, H. C. Howe, S. P. Hirshman, D. K. Lee, H. Arimoto, M. Hosokawa, H. Idei, S. Kubo, K. Matsuoka, K. Nishimura, S. Okamura, Y. Takeiri, Y. Takita and C. Takahashi, *Shafranov Shift in Low-Aspect-Ratio Heliotron / Torsatron CHS* ; Sep 1991

NIFS-111 R. Horiuchi, M. Uchida and T. Sato, *Simulation Study of Stepwise Relaxation in a Spheromak Plasma ;* Oct. 1991

NIFS-112 M. Sasao, Y. Okabe, A. Fujisawa, H. Iguchi, J. Fujita, H. Yamaoka and M. Wada, *Development of Negative Heavy Ion Sources for Plasma Potential Measurement* ; Oct. 1991

NIFS-113 S. Kawata and H. Nakashima, *Tritium Content of a DT Pellet in Inertial Confinement Fusion* ; Oct. 1991

NIFS-114 M. Okamoto, N. Nakajima and H. Sugama, *Plasma Parameter Estimations for the Large Helical Device Based on the Gyro-Reduced Bohm Scaling* ; Oct. 1991

NIFS-115 Y. Okabe, *Study of Au^- Production in a Plasma-Sputter Type Negative Ion Source* ; Oct. 1991

NIFS-116 M. Sakamoto, K. N. Sato, Y. Ogawa, K. Kawahata, S. Hirokura, S. Okajima, K. Adati, Y. Hamada, S. Hidekuma, K. Ida, Y. Kawasumi, M. Kojima, K. Masai, S. Morita, H. Takahashi, Y. Taniguchi, K. Toi and T. Tsuzuki, *Fast Cooling Phenomena with Ice Pellet Injection in the JIPP T-IIU Tokamak;* Oct. 1991

NIFS-117 K. Itoh, H. Sanuki and S. -I. Itoh, *Fast Ion Loss and Radial Electric Field in Wendelstein VII-Λ Stellarator*; Oct. 1991

NIFS-118 Y. Kondoh and Y. Hosaka, *Kernel Optimum Nearly-analytical Discretization (KOND) Method Applied to Parabolic Equations <<KOND-P Scheme>>:* Nov. 1991

NIFS-119 T. Yabe and T. Ishikawa, *Two- and Three-Dimensional Simulation Code for Radiation-Hydrodynamics in ICF*; Nov. 1991

NIFS-120 S. Kawata, M. Shiromoto and T. Teramoto, *Density-Carrying Particle Method for Fluid* ; Nov. 1991

NIFS-121 T. Ishikawa, P. Y. Wang, K. Wakui and T. Yabe, *A Method for the High-speed Generation of Random Numbers with Arbitrary Distributions;* Nov. 1991

NIFS-122 K. Yamazaki, H. Kaneko, Y. Taniguchi, O. Motojima and LHD Design *Group, Status of LHD Control System Design ; Dec. 1991*

NIFS-123 Y. Kondoh, *Relaxed State of Energy in Incompressible Fluid and Incompressible MHD Fluid* ; Dec. 1991

NIFS-124 K. Ida, S. Hidekuma, M. Kojima, Y. Miura, S. Tsuji, K. Hoshino, M. Mori, N. Suzuki, T. Yamauchi and JFT-2M Group, *Edge Poloidal Rotation Profiles of H-Mode Plasmas in the JFT-2M Tokamak ;* Dec. 1991

NIFS-125 H. Sugama and M. Wakatani, *Statistical Analysis of Anomalous Transport in Resistive Interchange Turbulence* ;Dec. 1991

NIFS-126 K. Narihara, *A Steady State Tokamak Operation by Use of Magnetic Monopoles* ; Dec. 1991

NIFS-127 K. Itoh, S. -I. Itoh and A. Fukuyama, *Energy Transport in the Steady State Plasma Sustained by DC Helicity Current Drive* ;Jan. 1992

NIFS-128 Y. Hamada, Y. Kawasumi, K. Masai, H. Iguchi, A. Fujisawa, JIPP T-IIU Group and Y. Abe, *New Hight Voltage Parallel Plate Analyzer* ; Jan. 1992

NIFS-129 K. Ida and T. Kato, *Line-Emission Cross Sections for the Charge-exchange Reaction between Fully Stripped Carbon and Atomic Hydrogen in Tokamak Plasma*; Jan. 1992

NIFS-130 T. Hayashi, A. Takei and T. Sato, *Magnetic Surface Breaking in 3D MHD Equilibria of l=2 Heliotron* ; Jan. 1992

NIFS-131 K. Itoh, K. Ichiguchi and S. -I. Itoh, *Beta Limit of Resistive Plasma in Torsatron/Heliotron* ; Feb. 1992

NIFS-132 K. Sato and F. Miyawaki, *Formation of Presheath and Current-Free Double Layer in a Two-Electron-Temperature Plasma* ; Feb. 1992

NIFS-133 T. Maruyama and S. Kawata, *Superposed-Laser Electron Acceleration* Feb. 1992

NIFS-134 Y. Miura, F. Okano, N. Suzuki, M. Mori, K. Hoshino, H. Maeda, T. Takizuka, JFT-2M Group, S.-I. Itoh and K. Itoh, *Rapid Change of Hydrogen Neutral Energy Distribution at L/H-Transition in JFT-2M H-mode ;* Feb. 1992

NIFS-135 H. Ji, H. Toyama, A. Fujisawa, S. Shinohara and K. Miyamoto *Fluctuation and Edge Current Sustainment in a Reversed-Field-Pinch;* Feb. 1992

NIFS-136 K. Sato and F. Miyawaki, *Heat Flow of a Two-Electron-Temperature Plasma through the Sheath in the Presence of Electron Emission;* Mar. 1992

NIFS-137 T. Hayashi, U. Schwenn and E. Strumberger, *Field Line Diversion Properties of Finite ß Helias Equilibria;* Mar. 1992

NIFS-138 T. Yamagishi, *Kinetic Approach to Long Wave Length Modes in Rotating Plasmas;* Mar. 1992

NIFS-139 K. Watanabe, N. Nakajima, M. Okamoto, Y. Nakamura and M. Wakatani, *Three-dimensional MHD Equilibrium in the Presence of Bootstrap Current for Large Helical Device (LHD);* Mar. 1992

NIFS-140 K. Itoh, S. -I. Itoh and A. Fukuyama, *Theory of Anomalous Transport in Toroidal Helical Plasmas;* Mar. 1992

NIFS-141 Y. Kondoh, *Internal Structures of Self-Organized Relaxed States and Self-Similar Decay Phase;* Mar. 1992

NIFS-142 U. Furukane, K. Sato, K. Takiyama and T. Oda, *Recombining Processes in a Cooling Plasma by Mixing of Initially Heated Gas;* Mar. 1992

NIFS-143 Y. Hamada, K. Masai, Y. Kawasumi, H. Iguchi, A. Fijisawa and JIPP T-IIU Group, *New Method of Error Elimination in Potential Profile Measurement of Tokamak Plasmas by High Voltage Heavy Ion Beam Probes;* Apr. 1992

NIFS-144 N. Ohyabu, N. Noda, Hantao Ji, H. Akao, K. Akaishi, T. Ono, H. Kaneko, T. Kawamura, Y. Kubota, S. Morimoto. A. Sagara, T. Watanabe, K. Yamazaki and O. Motojima, *Helical Divertor in the Large Helical Device;* May 1992

NIFS-145 K. Ohkubo and K. Matsumoto, *Coupling to the Lower Hybrid Waves with the Multijunction Grill;* May 1992

NIFS-146 K. Itoh, S. -I.Itoh, A. Fukuyama, S. Tsuji and Allan J. Lichtenberg, *A Model of Major Disruption in Tokamaks;* May 1992

NIFS-147 S. Sasaki, S. Takamura, M. Ueda, H. Iguchi, J. Fujita and K. Kadota, *Edge Plasma Density Reconstruction for Fast Monoenergetic Lithium Beam Probing;* May 1992

NIFS-148 N.Nakajima, C. Z. Cheng and M. Okamoto, *High-n Helicity-induced Shear Alfvén Eigenmodes;* May 1992